

170 Nanometer Nuclear Magnetic Resonance Imaging using Magnetic Resonance Force Microscopy

Kent R. Thurber^a Lee E. Harrell^b Doran D. Smith^{a,*}

^a*U.S. Army Research Laboratory, Adelphi, MD 20783.*

^b*Department of Physics, U.S. Military Academy, West Point, New York 10996.*

Abstract

We demonstrate one-dimensional nuclear magnetic resonance imaging of the semiconductor GaAs with 170 nanometer slice separation and resolve two regions of reduced nuclear spin polarization density separated by only 500 nanometers. This is achieved by force detection of the magnetic resonance, Magnetic Resonance Force Microscopy (MRFM), in combination with optical pumping to increase the nuclear spin polarization. Optical pumping of the GaAs creates spin polarization up to 12 times larger than the thermal nuclear spin polarization at 5 K and 4 T. The experiment is sensitive to sample volumes containing $\sim 4 \times 10^{11}$ $^{71}\text{Ga}/\sqrt{Hz}$. These results demonstrate the ability of force-detected magnetic resonance to apply magnetic resonance imaging to semiconductor devices and other nanostructures.

Key words: MRFM, force detected NMR, NMR microscopy, GaAs, optical pumping

PACS:

1 Introduction

Magnetic Resonance Imaging (MRI) has had many benefits to medicine and biology. However, the low sensitivity of the conventional inductive detection of nuclear magnetic moments has limited MRI to the micrometer scale and above[1,2,3]. The alternative technique of force detection of the magnetic resonance, Magnetic Resonance Force Microscopy (MRFM)[4,5], increases both

* Corresponding author.

Email address: ddsmith@arl.army.mil (Doran D. Smith).

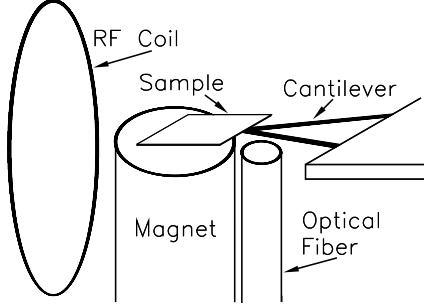


Fig. 1. Illustration of the MRFM probe head (approximately to scale). The magnet is iron wire 250 μm in diameter. The sample is doped GaAs $260 \times 180 \times 3 \mu\text{m}^3$ and attached to the Si_3N_4 cantilever with silver-filled epoxy. The 700 μm diameter copper RF coil generates the B_1 for the experiment and the single mode optical fiber is used to monitor the cantilever position.

the sensitivity and the resolution of MRI. Force detected NMR allows imaging with resolution well below one micrometer in solids, which opens up the application of MRI to semiconductor devices, thin films, and other nanostructures. In this article, we report force detection of $^{71,69}\text{Ga}$ and ^{75}As magnetic resonance in the semiconductor GaAs, in combination with optical pumping[6,7] to increase the nuclear spin polarization. We demonstrate one-dimensional nuclear magnetic resonance imaging of GaAs with 170 nanometer slice separation and resolve two regions of reduced nuclear spin polarization density separated by only 500 nanometers.

2 Materials and Methods

The force measured in a MRFM experiment is the force between two magnets: a small ferromagnet, and the nuclear (or electron) magnetic moments of the sample. Figure 1 shows an illustration of the MRFM probe head. In our experiment, the ferromagnet is a 250 μm diameter iron cylinder. The sample is a $\sim 260 \times 180 \times 3 \mu\text{m}^3$ layer of GaAs, doped at $0.6 \times 10^{18} \text{ cm}^{-3}$ Si and $2.0 \times 10^{18} \text{ cm}^{-3}$ Be. To detect the force between the sample and the ferromagnet, the GaAs sample is mounted with silver-filled epoxy on the end of a microcantilever and positioned 60 μm from the surface of the iron magnet. We used a Si_3N_4 cantilever[8] coated with 300 \AA Ti and 700 \AA Au on both sides for thermal conductivity (total spring constant k of the Au/Ti/ Si_3N_4 /Ti/Au sandwich $\sim 0.05 \text{ N/m}$). The loaded cantilever has a mechanical resonant frequency, $f_c = 490 \text{ Hz}$ and $Q = 75$ at 5 K in He exchange gas. The motion of the cantilever is observed with a fiber optic interferometer[9]. Further description of the cryostat and electronics is given in references [10,11].

The oscillation of the cantilever is driven by cyclic adiabatic rapid passage (ARP)[12]. The RF magnetic field ($\omega_{RF}/2\pi = 51.50 \text{ MHz}$) has a triangle wave

frequency modulation with peak-to-peak frequency width of $2\Omega/2\pi$, which flips the resonant nuclei at a frequency f_{ARP} . The RF magnetic field ($2B_1 \sim 0.4$ mT) is provided by a 700 μm diameter, 1 1/2 turn copper coil. The static magnetic field for resonance (3.96 T for ^{71}Ga at 51.50 MHz) is provided by the combination of an external superconducting magnet and the 250 μm diameter iron cylinder. The small size of the iron magnet results in a large magnetic field gradient (6000 T/m) at the center of the sample which provides the spatial selectivity for imaging. Only those spins in a total magnetic field satisfying the resonance condition will contribute to the signal.

Even at 5 K, the thermal spin polarization of the nuclei is rather small, 6×10^{-4} . To increase the nuclear spin polarization, we optically pump the GaAs sample[6,7,13]. An optical fiber shines circularly polarized light on the sample with a wavelength of 823 nm (near the bandgap of GaAs). Because of the GaAs band structure, the circularly polarized light creates electron-hole pairs with the electrons having 50% net polarization. The electrons then polarize the nuclei, through hyperfine interactions primarily at electronic defects (dynamic nuclear polarization). The optical pumping was typically done at 0.2 T external applied field because of the higher nuclear polarization achieved at low field. The magnetic field was then ramped up for the NMR measurements. Because of the long T_1 (21 ± 5 min)[11], very little spin polarization is lost in the roughly one minute required to change the magnetic field. The optical power (roughly 1400 W/m²) was kept low to avoid heating the sample. Since the sample is mounted at the end of a thin cantilever, thermal conductance away from the sample is low ($\approx 25 \mu\text{W/K}$).

3 Results

We observed all three naturally abundant nuclear isotopes in GaAs, ^{71}Ga , ^{69}Ga and ^{75}As , as shown in figure 2. The large width of the isotope peaks reflects the magnetic field gradient and the spatial extent of the sample. Each isotope peak is a 1D image of the nuclear spin polarization density of that isotope. For our cylindrical magnet, the imaging slices are shaped like a plate (thin with some curvature), as shown in cross-section in figure 3. The first signal at the lowest external magnetic field is from the bottom center of the sample. The signal grows rapidly with increasing external field as the slice volume extends deeper into the 3 μm thick sample. Once the tip of the imaging slice extends beyond the sample, the signal size declines slowly because of the reduced sample volume within the imaging slice. Using the observed maximum offset of the signal from the nominal resonance fields and the saturation magnetization for iron (2.18 T)[14], we can calculate the magnetic field gradient and the resonant slice geometry. For the imaging slice corresponding to the peak signal in figure 4 (\bullet , 3.388 T), the slices are separated by 170 nm with a total volume

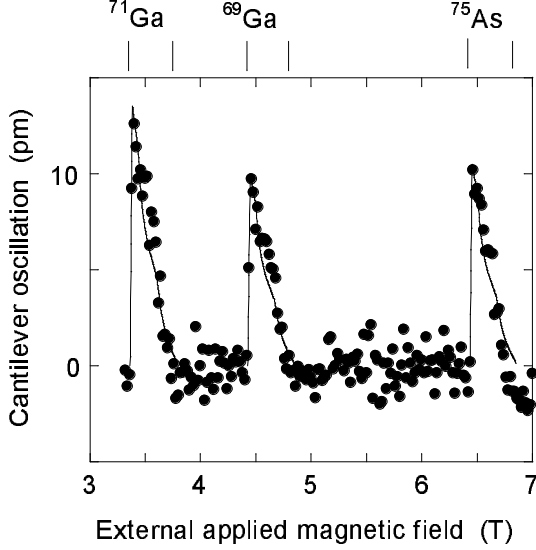


Fig. 2. Low-resolution 1D images of all three nuclear isotopes of the GaAs sample, ^{71}Ga , ^{69}Ga , and ^{75}As . Solid line is the calculated shape of the image. Data taken at $f_{ARP} = 33$ Hz (not cantilever mechanical resonance), $2\Omega/2\pi = 90$ kHz with 20 mT step size.

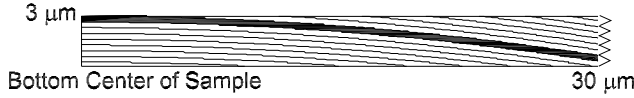


Fig. 3. Cross-section view of calculated geometry for 330 nm thick imaging slices. One slice shaded to correspond to filled data (\bullet) of figure 4.

of $600 \mu\text{m}^3$ and a magnetic field gradient of 6000 T/m. This volume contains 5×10^{12} ^{71}Ga nuclei with a signal to noise ratio (SNR) of $14 / \sqrt{Hz}$. Figure 4 shows single shot measurements of 2.5 or 5 seconds without any averaging. The good agreement between the leading edge of the data (figure 4 \circ) and the calculated signal (dotted line) confirms the calculated magnetic field gradient. The difference in the decline of the signal at higher external fields is caused by spatial variation in the optical pumping, which is most effective at the center of the sample. Figure 5 shows the nuclear spin polarization enhancement by optical pumping. Optical pumping at 0.2 T external field creates nuclear polarization as much as 12 times greater than the thermal polarization achieved at 5K and 4 T.

To demonstrate our ability to resolve structure in the nuclear spin polarization density, we want to see how close two planes of nuclear polarization can be and still be distinguished. To create contrast in our uniform GaAs sample, we sweep the magnetic field with constant frequency RF on, which inverts the nuclear polarization. During this sweep, we reduce the nuclear polarization in two closely spaced slices by exposing them to several seconds of cyclic ARP (see Fig. 6). Between the two slices of reduced polarization, we leave a third slice whose polarization is inverted along with the rest of the sample

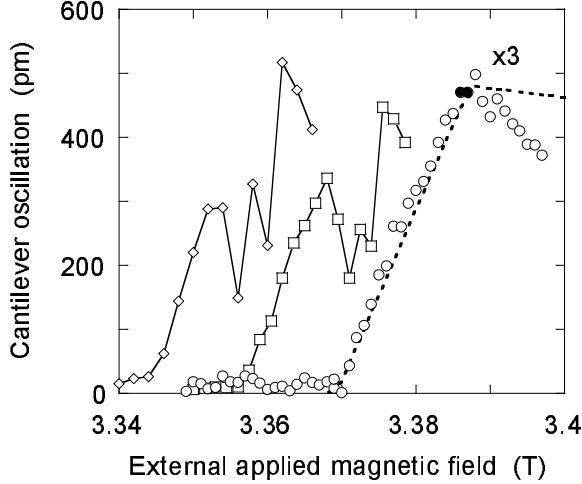


Fig. 4. High-resolution, optically pumped ^{71}Ga images. Open circle data (\circ , multiplied by 3) have a 170 nm imaging slice separation ($2\Omega/2\pi = 4$ kHz, 1 mT step). The dotted line represents calculations of the imaging slice volume from figure 3, and the two data points corresponding to the filled slice of figure 3 are also filled in. The resolution is demonstrated by destroying the spin polarization in two closely spaced slices and then imaging, for 670 nm (\diamond , offset by 0.03 Tesla) and 500 nm (\square , offset by 0.01 Tesla) separation between the two modified slices. (For 670 nm, $2\Omega/2\pi = 8$ kHz, 2 mT step; For 500 nm, $2\Omega/2\pi = 8$ kHz, 1.5 mT step.)

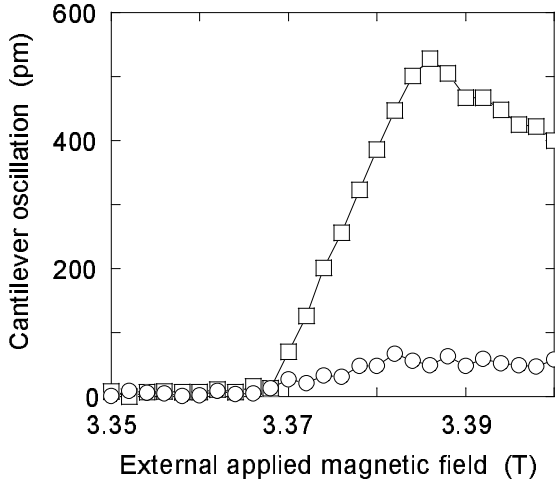


Fig. 5. Comparison of optically pumped (\square) and thermal (\circ) ^{71}Ga nuclear spin polarization ($2\Omega/2\pi = 8$ kHz, 2 mT step).

region, but has nominally unaltered polarization magnitude. Following this, we measure the resulting polarization. As shown in figure 4, we can resolve the nuclear spin polarization signal from two slices separated by only 500 nm. This is only an upper limit on the resolution of this instrument because we are doing cyclic ARP on each slice twice: first to reduce the spin polarization to provide contrast and then a second time to measure the image. Some of the blurring of the slices occurs in the creation of the spin-polarization contrast

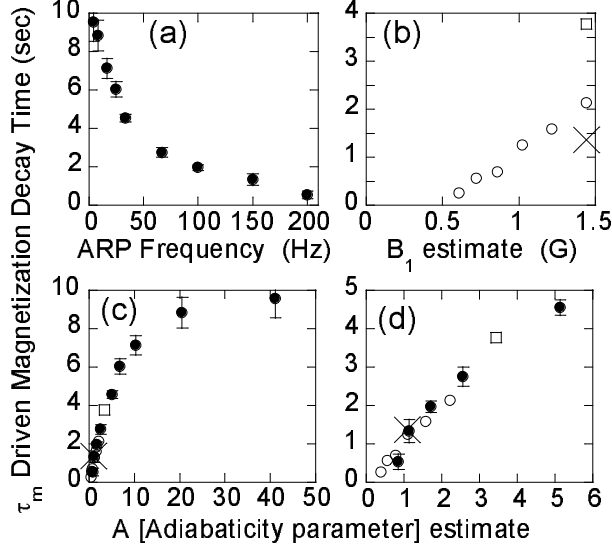


Fig. 6. (a) \bullet Decay time constant, τ_m , of ARP driven nuclear magnetization as a function of ARP frequency, f_{ARP} . (^{69}Ga , $2\Omega/2\pi = 40$ kHz) (b) Decay time as a function of B_1 and γ . (\circ ^{69}Ga , \square ^{71}Ga , \times ^{75}As , $f_{ARP} = 33$ Hz, $2\Omega/2\pi = 94$ kHz) (c) Decay time as a function of adiabatic parameter, A . Data of parts a and b combined. (d) Expanded view of low A region of part c.

before imaging.

4 Discussion

The thickness of the spatial imaging slices in our experiment is primarily determined by the frequency width of the ARP relative to the magnetic field gradient. In this experiment, the highest resolution data was taken with the peak-to-peak frequency modulation of the adiabatic rapid passage, $2\Omega/2\pi = 4$ kHz (equivalent to 0.31 mT for ^{71}Ga) and the data points were taken every 1 mT. The data points are thus separated by the magnetic field step size divided by the field gradient, $1 \text{ mT} / (6000 \text{ T/m}) = 170 \text{ nm}$. We found that reducing the ARP modulation further rapidly reduced the SNR. This is logical because there are multiple effects which smear the spatial resolution at the 0.1 mT level. First, there is $B_1 \sim 0.2$ mT, which determines the width of the resonance. Assuming that the adiabatic condition is met during the passage and that relaxation processes can be neglected, the modulation of the z-axis magnetization is[5]

$$M_z(t) = M_0(\mathbf{r}) \frac{\gamma\delta B(\mathbf{r}) - \Omega t}{\sqrt{[\gamma\delta B(\mathbf{r}) - \Omega t]^2 + (\gamma B_1)^2}} \quad (1)$$

where $M_0(\mathbf{r})$ is the nuclear polarization at position \mathbf{r} , γ is the nuclear gyromagnetic ratio ($\gamma = 2\pi \times 13.0$ MHz/T for ^{71}Ga), $\gamma\delta B(\mathbf{r}) = \gamma B(\mathbf{r}) - \omega_{RF}$ is the offset field from resonance, and $B(\mathbf{r})$ is the total magnetic field at a position \mathbf{r} in the sample. The time variable, t , varies from -1 to +1 during the adiabatic passage. This equation is correct for the spin 3/2 nuclei in this experiment, $^{71,69}\text{Ga}$ and ^{75}As , as long as the quadrupole coupling is negligible. In this equation, B_1 has two effects. Large B_1 increases the width of the resonance, thus modulating spins further from the center of the slice. Large B_1 also increases the frequency width, Ω , required to fully modulate the spins. A small γB_1 relative to Ω is required to have the slice width depend primarily on Ω . Having $\gamma B_1 < \Omega$ provides a large modulation of the spins and sharper edges of the imaging slice.

However, B_1 in combination with Ω and f_{ARP} also determines the adiabaticity of the rapid passages. To have adiabatic passages requires the adiabatic parameter A ,

$$A = \frac{(\gamma B_1)^2}{4\Omega f_{ARP}} \gg 1 \quad (2)$$

This equation clearly favors large B_1 . Figure 6 shows the effect of f_{ARP} , B_1 , and γ on the decay time τ_m of the nuclear magnetization driven by ARP. The available measurement time becomes significant for $B_1 > 0.05$ mT. As a result, the experiment requires both $\gamma B_1 \lesssim \Omega$ and $(\gamma B_1)^2 \gg 4\Omega f_{ARP}$. If we take $\gamma B_1 = \Omega$, we can simplify these equations to see that we require roughly $4f_{ARP} \ll \gamma B_1 \lesssim \Omega$. Since minimizing Ω gives us the highest resolution, we also want to minimize f_{ARP} . In order to use the Q enhancement of the mechanical cantilever resonance to amplify the signal relative to measurement noise, we want $f_{ARP} = f_c$. In this experiment, a rather large sample was deliberately used to mass load the cantilever and lower its resonant frequency, f_c .

Besides these considerations for the cyclic ARP measurement, sample properties also can provide limits to the current experimental resolution. The intrinsic linewidth of ^{71}Ga in GaAs is about 0.2 mT[13]. As can be seen in figure 6(c), even if the rapid passage is very adiabatic, the driven magnetization still decays in about 10 seconds. Even for an adiabatic passage, the time spent on resonance is limited by the spin lock time constant, $T_{1\rho}$. Another effect which could limit spatial resolution is spin diffusion. The effect of spin diffusion was not seen in this experiment. Spin diffusion should become important as the resolution is further increased based on the expected spin diffusion constants, ($D = 10^{-13}$ cm²/s for ^{75}As [7]).

The current resolution is limited by the size of B_1 and linewidth relative to the magnetic field gradient, not the sensitivity. There is room for improvement of the resolution (and the sensitivity, also) by decreasing the size of the fer-

romagnetic particle, which increases the magnetic field gradient. Higher field gradients have already been used for ESR experiments[15]. For detailed comparisons of mechanical versus inductive detection of magnetic resonance, see references [16,17].

5 Conclusions

We have used force-detected magnetic resonance to image GaAs in one-dimension with 170 nanometer slice spacing and resolve two regions of reduced nuclear spin polarization density separated by only 500 nanometers. We also demonstrated the combination of force-detected magnetic resonance with optical pumping to increase nuclear spin polarization. We can detect volumes containing $\sim 4 \times 10^{11}$ $^{71}\text{Ga}/\sqrt{Hz}$ with orders of magnitude of further improvement expected. This enables NMR of very small samples and high resolution imaging. We envision wide ranging application of force-detected magnetic resonance to study many types of samples including biological membranes and molecules, surfaces and thin films, and semiconductor materials and devices.

6 Acknowledgements

This work was partially supported by the DARPA Defense Science Office Spins in Semiconductors program. The sample was grown and processed by Peter Newman and Monica Taysing-Lara. The authors would like to thank John A. Marohn and John Sidles for many helpful discussions.

References

- [1] S.-C. Lee, *et al.*, One micrometer resolution NMR microscopy, *J. Magn. Reson.* **150**, 207 (2001).
- [2] D. A. Seeber, L. Ciobanu, C. H. Pennington, Advances toward MR microscopy of single biological cells, *Appl. Magn. Reson.* **22**, 139 (2002).
- [3] K. R. Minard and R. A. Wind, Picoliter ^1H NMR spectroscopy, *J. Magn. Reson.* **154**, 336 (2002).
- [4] J. A. Sidles, Noninductive detection of single-proton magnetic resonance, *Appl. Phys. Lett.* **58**, 2854 (1991).

- [5] O. Züger, S. T. Hoen, C. S. Yannoni, D. Rugar, Three-dimensional imaging with a nuclear magnetic resonance force microscope, *J. Appl. Phys.* **79**, 1881 (1996).
- [6] G. Lampel, Nuclear dynamic polarization by optical electronic saturation and optical pumping in semiconductors, *Phys. Rev. Lett.* **20**, 491 (1968).
- [7] D. Paget, Optical detection of NMR in high-purity GaAs: Direct study of the relaxation of nuclei close to shallow donors, *Phys. Rev. B* **25**, 4444 (1982).
- [8] MLCT-NOHW Microcantilevers, Park Scientific Instruments, Sunnyvale, CA.
- [9] K. J. Bruland, J. L. Garbini, W. M. Dougherty, S. H. Chao, and S. E. Jensen, Thermal tuning of a fiber-optic interferometer for maximum sensitivity, *Rev. Sci. Instrum.* **70**, 3542 (1999).
- [10] D. D. Smith, J. A. Marohn, and L. E. Harrell, Detailed description of a compact cryogenic magnetic resonance force microscope, *Rev. Sci. Instrum.* **72**, 2080 (2001).
- [11] K. R. Thurber, L. E. Harrell, R. Fainchtein, D. D. Smith, Spin polarization contrast observed in GaAs by force-detected nuclear magnetic resonance, *Appl. Phys. Lett.* **80**, 1794 (2002).
- [12] C. P. Slichter, "Principles of Magnetic Resonance," 3rd edition, Springer-Verlag, Berlin, 1990, pp. 22-25.
- [13] S. E. Barrett, R. Tycko, L. N. Pfeiffer, and K. W. West, Directly detected nuclear magnetic resonance of optically pumped GaAs quantum wells, *Phys. Rev. Lett.* **72**, 1368 (1994).
- [14] R. M. Bozorth, "Ferromagnetism," Van Nostrand, New York, 1951, pg. 54.
- [15] K. J. Bruland, W. M. Dougherty, J. L. Garbini, J. A. Sidles, and S. H. Chao, Force-detected magnetic resonance in a field gradient of 250000 Tesla per meter, *Appl. Phys. Lett.* **73**, 3159 (1998).
- [16] J. A. Sidles, and D. Rugar, Signal-to-noise ratios in inductive and mechanical detection of magnetic resonance, *Phys. Rev. Lett.* **70**, 3506 (1993).
- [17] G. M. Leskowitz, L. A. Madsen, and D. P. Weitekamp, Force-detected magnetic resonance without field gradients, *Solid State Nucl. Magn. Reson.* **11**, 73 (1998).